

Journal of Biomedical Optics

BiomedicalOptics.SPIEDigitalLibrary.org

Intraoperative imaging of pediatric vocal fold lesions using optical coherence tomography

Fouzi Benboujja
Jordan A. Garcia
Kathy Beaudette
Mathias Strupler
Christopher J. Hartnick
Caroline Boudoux

Intraoperative imaging of pediatric vocal fold lesions using optical coherence tomography

Fouzi Benboujja,^a Jordan A. Garcia,^b Kathy Beaudette,^a Mathias Strupler,^a Christopher J. Hartnick,^b and Caroline Boudoux^{a,b,*}

^aPolytechnique Montréal, Department of Engineering Physics, P.O. Box 6079 Station Centre-Ville, Montréal, Quebec H3C 3A7, Canada

^bHarvard Medical School, Massachusetts Eye and Ear Infirmary, Department of Otolaryngology, 243 Charles Street, Boston, Massachusetts 02114, United States

Abstract. Optical coherence tomography (OCT) has been previously identified as a promising tool for exploring laryngeal pathologies in adults. Here, we present an OCT handheld probe dedicated to imaging the unique geometry involved in pediatric laryngoscopy. A vertical cavity surface emitting laser-based wavelength-swept OCT system operating at 60 frames per second was coupled to the probe to acquire three-dimensional (3-D) volumes *in vivo*. In order to evaluate the performance of the proposed probe and system, we imaged pediatric vocal fold lesions of patients going under direct laryngoscopy. Through this *in vivo* study, we extracted OCT features characterizing each pediatric vocal fold lesion, which shows a great potential for noninvasive laryngeal lesion discrimination. We believe OCT vocal fold examination in 3-D will result in improved knowledge of the pediatric anatomy and could aid in managing pediatric laryngeal diseases. © The Authors. Published by SPIE under a Creative Commons Attribution 3.0 Unported License. Distribution or reproduction of this work in whole or in part requires full attribution of the original publication, including its DOI. [DOI: [10.1117/1.JBO.21.1.016007](https://doi.org/10.1117/1.JBO.21.1.016007)]

Keywords: optical coherence tomography; vocal fold; pediatric; benign laryngeal lesions.

Paper 150709 received Oct. 26, 2015; accepted for publication Dec. 15, 2015; published online Jan. 18, 2016.

1 Introduction

Voice production is a complex process, which can be considerably affected by the presence of benign lesions. Approximately 6% to 9% of children^{1,2} and nearly one-third of the population will be affected by a voice disorder during their lifetimes.³ In children, benign lesions like nodules, polyps, and cysts are common causes of voice hoarseness. Clinical evaluation of voice hoarseness includes obtaining the patient's medical history, performing perceptual voice analysis, and inspecting the larynx⁴ using a nasolaryngoscope in clinic or a rigid bronchoscope in the operating room.⁵ Otolaryngologists base their diagnosis and treatment strategy on visual inspection of the motion of the mucosa, glottal closure, and the appearance of superficial blood vessels.^{6,7}

Although a magnified view of the vocal folds through endoscopy is very useful to clinicians, images are difficult to interpret. The superficial appearance (morphology, coloration, and vascularization) of laryngeal structures is sensitive to lighting conditions and camera angle.⁸ Furthermore, most diseases arise below the epithelial layer⁷ and are therefore invisible using superficial imaging techniques.⁹ Overall, it remains challenging to differentiate these subepithelial lesions clinically and histologically.¹⁰⁻¹² For instance, the outer surface of nodules and cysts is relatively similar as they macroscopically appear as a thickening of the epithelial layer. To this day, defining characteristic features of benign lesions remains an active area of investigation,¹³ as treatment strategies differ for each lesion type.

Radiological imaging modalities such as magnetic resonance imaging, computed tomography, x-rays, and ultrasound

are unfortunately unable to properly assess the vocal fold mucosal structure. Their resolution is insufficient for microscopic features and their contrast in this context is low. Despite the associated risks, the only option to determine the type and extent of laryngeal disease remains surgical biopsies. Although biopsy followed by histology is the clinical gold standard, it produces large amounts of false-negative results due to sampling errors, and therefore, not suited to analyze large surfaces. More importantly, biopsy of the vocal fold can cause scarring, which may negatively affect voice quality.¹⁴ Therefore, noninvasive assessment of the type and extent of a lesion could substantially improve the outcomes of therapeutic procedures for the pediatric population.

Recently, several optical imaging technologies have been evaluated as potential tools for assessing the microanatomy of the vocal fold.¹⁵⁻¹⁷ Among these, optical coherence tomography (OCT)¹⁸ was identified as an appealing noninvasive imaging technology for laryngeal diagnoses in pediatric laryngology. OCT provides cross-sectional imaging of biological tissues with micrometer scale resolution, millimeter scale field-of-view, and imaging speed compatible with three-dimensional (3-D) imaging.

Several studies investigated the use of OCT in laryngology. Applications range from monitoring laser surgery of laryngeal carcinoma¹⁹ to the optical characterization of the unique layered structure of the vocal fold.^{20,21} OCT was also used to investigate lesions of the upper aerodigestive tract in adults.^{22,23} Despite numerous *in vivo* OCT studies focused on laryngeal diseases,^{22,24-29} very few have explored using OCT in the pediatric population. *In vivo* OCT imaging was used to examine the upper digestive tract including various pathologies of the pediatric airway microanatomy using time-domain OCT (TD-OCT),²⁸ but did not specifically focus on vocal fold lesions. Additionally,

*Address all correspondence to: Caroline Boudoux, E-mail: caroline.boudoux@polymtl.ca

acquisition speed (a few frames per seconds) and sensitivity of TD-OCT systems confined the study to two-dimensional (2-D) imaging which might not be sufficient to grasp the complex spatial extent of some vocal fold pathologies. Recent studies using Fourier domain systems have investigated the detection of subglottic stenosis on neonates.^{29,30}

Pediatric laryngology brings its own set of challenges, as probe dimensions need to meet specific requirements to allow imaging the youngest patients without obstructing their airways. Additionally, bilateral vocal fold imaging implies rapid acquisition rates to avoid motion artifacts and necessitates a probe ergonomics to allow rapid and precise positioning of its tip to the appropriate region-of-interest.

We present an OCT-based handheld probe specifically adapted to the pediatric population, for *in vivo* imaging of vocal fold lesions. The probe allows for rapid 3-D imaging of the strike zone area (i.e., the contact area of the two vocal cords during phonation) where lesions are most likely to occur. The probe is coupled to a mobile cart, allowing easy integration into the clinical flow. We herein present *in vivo* OCT images of benign lesions acquired with this system and demonstrate the added advantage of 3-D OCT imaging for lesion discrimination and margins assessment.

2 Materials and Methods

In this section, we present the clinical OCT system and probe used for *in vivo* evaluation of pediatric vocal folds.

2.1 Study Design

Prior to our *in vivo* study, we imaged 20 adult cadaveric vocal fold specimens with OCT and compared images with corresponding histology sections for both normal and pathological cases. Results from this *ex vivo* study were used as an atlas to guide *in vivo* observations. For each *ex vivo* specimen, a full OCT scan was performed from the anterior to the posterior segment of the vocal cord using an OCT system described in Sec. 2.2. Axial and lateral resolutions of the benchtop system are 12 and 25 μm , respectively, and the incident power on the sample is ~ 15 mW. The field-of-view is 10-mm long, 2-mm wide, and 3-mm deep and includes, in addition to the true vocal fold, some adjacent structures such as a portion of the ventricle, which serves as a reference point for comparison with histology. For correspondence between OCT and histology images, each end of the vocal fold (i.e., in the inferior–superior axis) was marked with India ink, which is visible in both OCT images and histology sections. Immediately after the OCT imaging, the sample was placed in a solution of formaldehyde for fixation and was processed for histological evaluation using hematoxylin–eosin (H&E) staining. Throughout this paper, OCT images are presented using a logarithmic scale of the back-scattered intensity.

Following the *ex vivo* study, we performed *in vivo* OCT imaging on 20 children ranging from 3 months to 16 years of age. Prior to the procedure, description and consent forms were given to parents and children. Approval of this study was obtained from patient subjects and the Massachusetts Eye and Ear Infirmary (Boston, Massachusetts) Institutional Review Board (IRB: 208399). Pediatric candidates were recruited from patients undergoing bronchoscopy or minor surgery at Massachusetts Eye Ear Infirmary (Boston, Massachusetts). Prior to imaging, patients were put under general anesthesia and prepared for suspension microlaryngoscopy. The OCT handheld probe

was first inserted into the oral cavity and lightly brought into contact with the region-of-interest on the vocal cord. This was done under direct visualization or under video laryngoscopy guidance. Once the target area was reached, 3-D recording was triggered. OCT acquisition was performed on the left and right vocal folds when possible. Each volume (2 mm \times 2 mm \times 7 mm) was acquired within 18 s. Immediately after OCT imaging, the scheduled airway procedure was performed.

2.2 Optical Coherence Tomography System

Proper visualization of pediatric vocal fold lesions during standard laryngoscopy examination imposes stringent constraints on the OCT system and its imaging probe. Rapid acquisition is necessary to avoid motion artifacts, allowing for 3-D imaging while minimizing the time patients remain under general anesthesia. Probe design must allow for imaging of a wide range of anatomical dimensions as the larynx size and vocal fold length increase during development. The complete imaging system must finally be robust and portable for repetitive use in the surgical suite.

Figure 1(a) shows a schematic diagram of the OCT system, which consists of a swept source system (OCS1310V1 Thorlabs, Newton, New Jersey) modified to accommodate an external reference arm [Fig. 1(b)] matching our custom handheld probe [Fig. 1(c)].

2.2.1 Optical coherence tomography source

The OCT source is a vertical cavity surface emitting laser-based wavelength-swept laser³¹ centered at 1310 nm for enhanced imaging depth. Its 10-dB bandwidth is 117-nm wide, resulting in an axial resolution of 16 μm in air and 12 μm in tissue. Its A-line acquisition rate (100 k A-lines/s) allows for an imaging speed of 60 images/s (for 1040 A-lines of 1040 pixels), and its average output power is 30 mW. This source provides a long coherence length, which allows for an imaging range of up to 10 mm; a feature particularly helpful for imaging lesions presenting with a severe deformation of the epithelium.

2.2.2 Reference arm

Figure 1(b) shows a schematic diagram of an external reference arm used to accommodate our custom probe. The reference arm was designed to compensate for the dispersion induced by the probe's optics to avoid axial resolution degradation. In the reference arm, the collimated light propagates through three 2.7-mm diameter gradient-index (GRIN) lenses for a total length of 317 mm. This assembly acts as an optical relay, which focuses light on a mirror. An iris is used to optimize the signal-to-noise ratio in the acquired images.

2.2.3 Optical coherence tomography handheld probe

Intraoperative laryngeal evaluation justifies the use of a rigid handheld probe, which in turn allows for precise placement at the strike zone for 3-D imaging. Figure 1(c) shows a schematic diagram of the probe. The probe design allows for optimal focus depth adjustment inside the tissue by properly adjusting the objective lens distance with the first GRIN lens interface. In order to achieve optimal resolution of the lamina propria, light was focused at a distance of 1 mm from the distal tip of the probe. This configuration is achieved with the following optical design: collimated light is focused with a 19-mm focal length

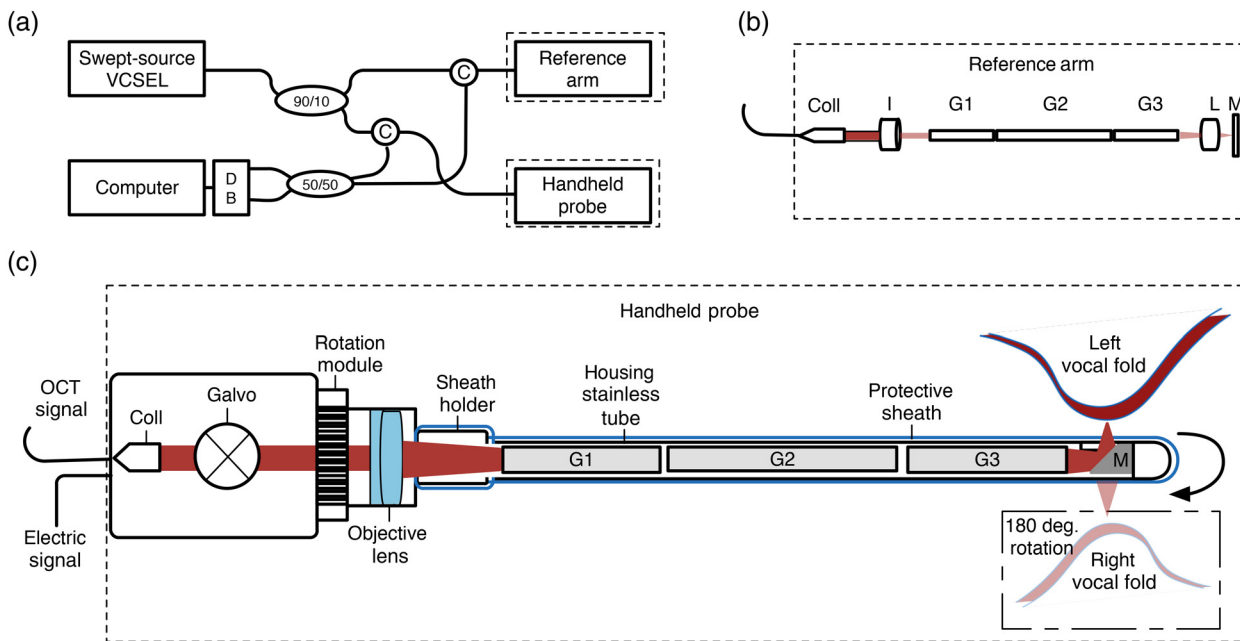


Fig. 1 (a) Schematic diagram of the OCT imaging system and details of its (b) reference and (c) imaging arms. DB, dual-balanced detector; C, circulator; Coll, collimator; I, iris; G1 and G3, 95-mm long GRIN lens; G2, 127-mm long GRIN lens; L, 19-mm focal length lens; Galvo, galvanometers; M, mirror; and objective lens, 19-mm focal length.

lens (Thorlabs, AC127-019-C) inside a GRIN lens assembly. The assembly has three GRIN lenses (Gradient Lens Corporation, Rochester, New York) of 2.7 mm in diameter and separated by two 1-mm thick spacers. In this configuration, the GRIN lenses assembly acts as an optical relay. A 3-mm diameter, 45-deg rod mirror (Edmund Optics, 54-093, aluminum coating) is mounted at the probe tip with optical-grade ultraviolet glue (Norland Optical Adhesive 84), reflecting light on the edge of the vocal fold. The mirror length was polished down to 3.5 mm to limit the offset between the imaging window and the distal end of the probe for easier alignment.

Each optical interface (collimator, objective lens, GRIN lenses) is coated with an infrared antireflection coating to minimize back reflection. The GRIN lenses are inserted into a stainless steel tube (2.9-mm inner diameter and 0.8-mm thick) to increase probe rigidity resulting in a 324-mm long final assembly. This length is adequate for a variety of larynx sizes (i.e., 3 months to 17 years of age). The size of the probe is also compatible with a standard disposable translucent sterile sheath (Slide-ON Endosheath, Medtronic, Jacksonville, Florida), which allows for rapid system setup in between patients. The outer tube is graduated in millimeters [Fig. 2(b)] to help with orientation and estimating lesion dimensions. Probe tips can be interchanged easily using a chuck and collet mechanism as shown in Fig. 2(c). Table 1 summarizes the characteristics of the probe.

Volumetric data acquisition is obtained with a fast 2-D scanning mechanism—the third dimensions being inherent to OCT imaging. Lateral raster scan is implemented with two 3-mm mirror-mounted galvanometers (6215H Cambridge Technology). A rotation mechanism was also added to the handheld probe [Fig. 2(b)] to allow a symmetric analysis of the vocal cords (i.e., imaging of the right and left vocal cords at the same anterior–posterior position) and for imaging irregular shapes such as nodules and cysts. This additional degree of freedom allows for the surgeon's hand to remain still in a neutral position and only

rotate the viewing window such that the optimum angle for a lesion can be reached. A 0-deg angle aligns the OCT beam such that a scan of the right vocal fold can be done perpendicularly to the strike zone (i.e., coronal plane) from a superior to inferior position. By providing a scan angle guideline, we added stability and increased the repeatability of the procedure in the surgical suite.

The complete system is installed on a conventional surgery cart (GoKart 9601A, Karl Storz Endoscopy, El Segundo, California) [Fig. 2(c)]. The self-contained system is robust to vibrations and can easily be moved from the laboratory to the surgical room. The acquisition computer is equipped with a high-speed acquisition board (ATS9350 Alazar Technologies, Pointe-Claire, Canada). The signal is sampled at 500 MHz with a resolution of 12 bits and is then saved to a hard disk. OCT Software ThorImage (Version 4.2, Newton, New Jersey) is used during acquisition. Postprocessing is done using customized software (C++, Qt) to extract and analyze raw images.

3 Vocal Fold Imaging

3.1 Ex Vivo Imaging

Figure 3(a) shows a representative OCT cross section of the normal adult cadaveric aerodigestive track spanning the subglottic and supraglottic areas along the midmembranous portion of the vocal fold. The first layer represents the epithelium (Ep) and can be clearly distinguished from the underlying lamina propria (Lp). The lamina propria is always seen as a hyperluciscent (highly scattering) region regardless the location along the aerodigestive track (subglottic, glottis, or supraglottic). In the subglottic area, the lamina propria is rich in seromucinous glands (G). As shown in the OCT images, these glands appear as hypoluciscent (weakly scattering) and are distributed at different locations within the lamina propria in the subglottic region. This can be seen throughout volumes acquired (Video 1). In the true vocal

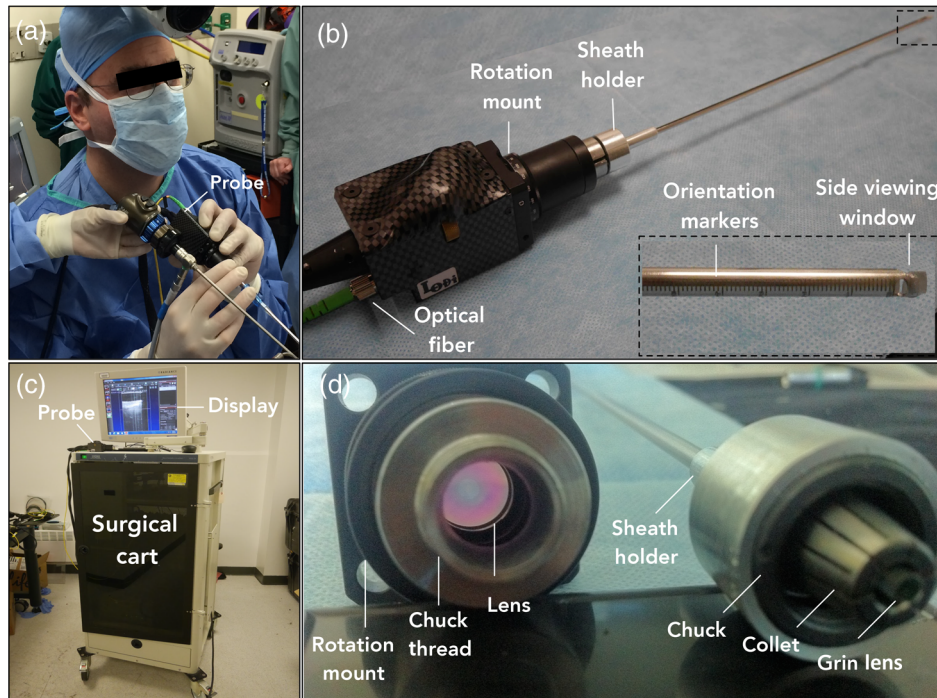


Fig. 2 (a) *In vivo* OCT imaging with the handheld probe during suspension microlaryngoscopy. (b) Handheld probe with inset showing graduation marks at the probe tip. (c) Intraoperative OCT system mounted in a surgical cart used for vocal fold imaging. (d) The docking mechanism allowing for rapid interchange of probe tips in between patients.

Table 1 OCT probe technical specifications.

Specifications	Values
Lateral resolution (FWHM)	25 μm
Axial resolution ($1/e^2$)	12 μm
Field-of-view	2 mm
A-line rate	100 kHz
Laser power at sample	≤ 5 mW
Probe diameter	3.7 mm
Probe length	324 mm

fold, there are no such subepithelial glandular structures and the signal decays down to the vocalis muscle (Ms). Distinctive signal intensities are observed within the lamina propria suggestive of the layered structure described in Ref. 32. The corresponding histological section is shown in Fig. 3(b).

The epithelium layer thickness along the aerodigestive track is not uniform, which can be attributed to a change in the epithelial cell type. The transition is gradual from a very thin layer (40 to 75 μm) of squamous stratified epithelial cells (Ss) at the strike zone, to a thicker pseudostratified ciliated epithelium (Ps) layer (75 to 120 μm) inferior to the strike zone. This change in thickness is visible in both OCT and histology sections [Figs. 3(a) and 3(b)].

Figure 4 shows lesions imaged *ex vivo* under OCT with the corresponding histology section. Fiducial markers (M1–M2) used for comparison are visible both in the OCT images and

the histology sections. The epithelium covering the nodule area [Fig. 4(a)] is thicker than the epithelium layer found inferior or superior. Such localized thickening was not seen in our control patients. The basement membrane appears irregular, curved with some invaginations, which might indicate signs of epithelial hyperplasia.³³ In the superficial region of the lamina propria, an increased backscattered signal is observed compared to surrounding tissue, which may be an indication of edema and fibrosis, commonly found in nodules.³³

Figures 4(c) and 4(d) show a mucus retention multiloculated pseudocyst, beneath the epithelial layer, that occupies a significant space in the lamina propria. The cyst structure and type were confirmed by histopathology, shown in Fig. 4(d). The lesion area is almost circular, partitioned and mostly filled with aqueous material. Consequently, the OCT image displays a very delineated void region. As seen in the histology section [Fig. 4(d)], the cyst lining is not epithelized. Its multiloculated structure is clearly visible in both OCT and histology sections. The 3-D-OCT sequence (Video 2) allows evaluating the full extent of the cyst region.

Visualization of volumetric OCT data allows qualitative and quantitative information to be extracted such as lesions' symmetry and dimension. Figure 5 shows a 3-D rendering (Amira, FEI Visualization Science Group, Burlington, Massachusetts) of nodule [Fig. 5(a)] and cyst [Fig. 5(c)] showed previously along with their respective zoomed region [Figs. 5(b) and 5(d)].

Lesions are located and confined to a few millimeters away from the free edge of the true vocal fold (i.e., away from the ventricle). The dimensions of nodule and volume occupied by pseudocyst are evaluated after segmenting the 3-D data set. The nodule expands by 1.5 mm in the anterior–posterior and the superior–inferior axes. The cyst is not symmetrical and expands

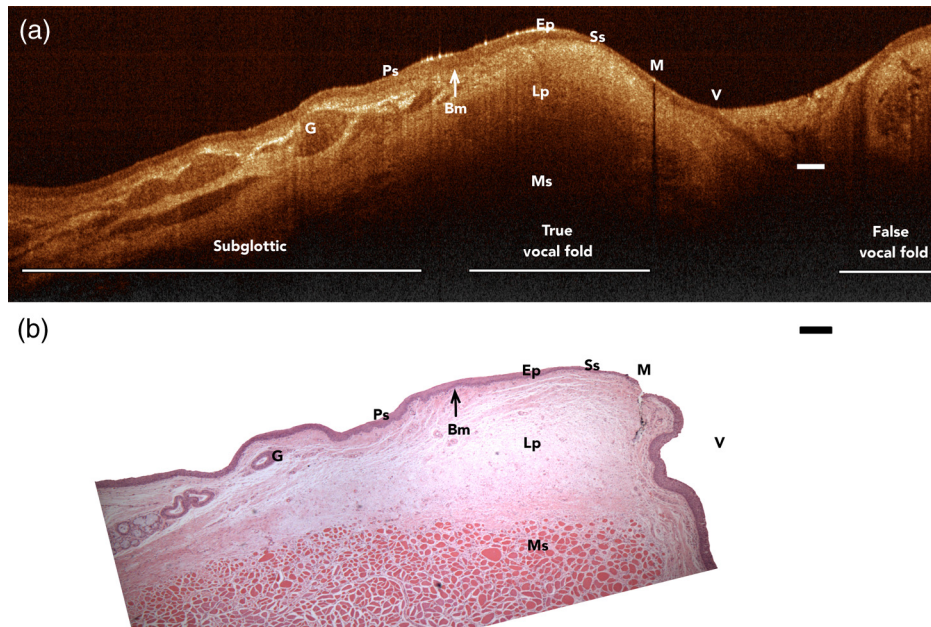


Fig. 3 (a) OCT cross section of a normal aerodigestive tract and (b) corresponding histology section (100× H&E staining) of an adult cadaveric sample. G, serous gland; Ps, pseudostratified ciliated epithelium; Bm, basement membrane; Ep, epithelial layer; Lp, lamina propria; Ms, muscle; Ss, squamous stratified epithelium; M, fiducial mark; and V, ventricle. Scale bars: 200 μ m. Video 1 shows a C-scan fly-through of a control 3-D OCT data set. (Video 1, MOV size 7 MB [URL: <http://dx.doi.org/10.1117/1.JBO.21.1.016007.1>]).

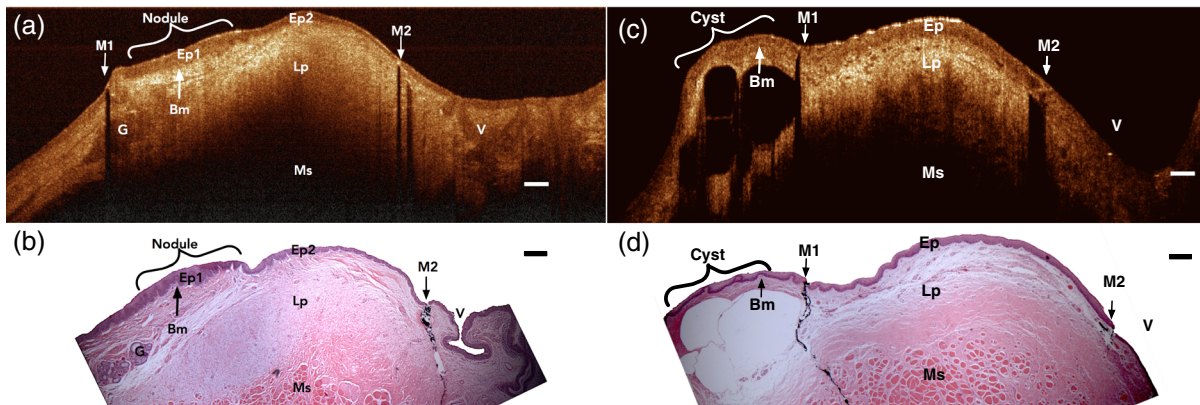


Fig. 4 OCT cross section of a nodule [(a) adult cadaveric specimen] with corresponding histological section [(b) H&E staining, 100×]. OCT cross section of a mucus retention pseudocyst [(c) adult cadaveric specimen] with corresponding histological section [(d) H&E staining, 100×]. Ep, epithelial layer; Lp, lamina propria; V, ventricle; G, serous gland; M1 and M2, fiducial markers; Bm, basement membrane; Ms, muscle. Scale bars: 200 μ m. Video 2 shows a fly-through 3-D OCT data set of the same cyst. (Video 2, MOV size 6 MB [URL: <http://dx.doi.org/10.1117/1.JBO.21.1.016007.2>]).

on 1.8 mm on the superior–inferior axis and 1.5 mm on the anterior–posterior axis and 1-mm deep in the lamina propria.

The 3-D projections shown in Fig. 5 highlight zones of distinctive signal intensities (Lp1–Lp2) visible within the lamina propria, which was also observed in the normal vocal fold in Fig. 3(a).

3.2 In Vivo Imaging

We performed OCT imaging on 20 pediatric patients, among which 10 showed lesions. All imaging sessions yielded useful

data aside from some back reflection artifacts from the sterile protective sheath.

Figure 6 shows images of the vocal folds of a healthy 9-year-old male. Intraoperative endoscopy [Fig. 6(a)] shows the probe in contact with the left vocal cord. Probe placement at the strike zone was achieved for every case using the method depicted in Video 3. Initially, the probe tip is placed inferior to the edge of the vocal fold in the subglottic region. The imaging window is placed perpendicular to the free edge in the midmembranous portion of the vocal fold. Under OCT guidance, the probe tip is slowly moved superiorly. Real-time 2-D imaging is used to orient the probe tip to the strike zone for 3-D volume acquisition.

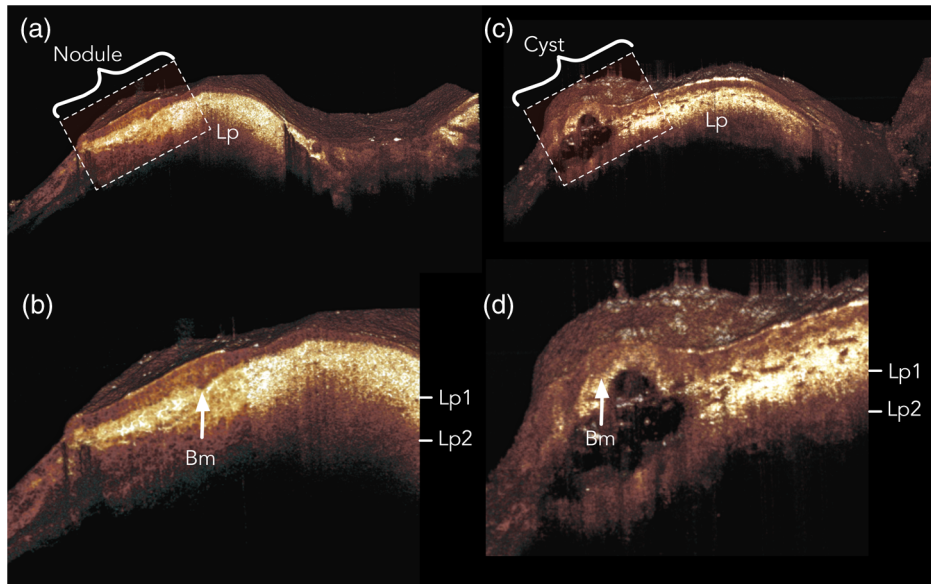


Fig. 5 *Ex vivo* volumetric rendering of (a) adult vocal fold nodule (inset shown in b) and (c) of a mucus retention cyst (inset shown in d). BM, basement membrane; Lp, lamina propria; Lp1–Lp2, lamina propria with zones of varying optical intensities.

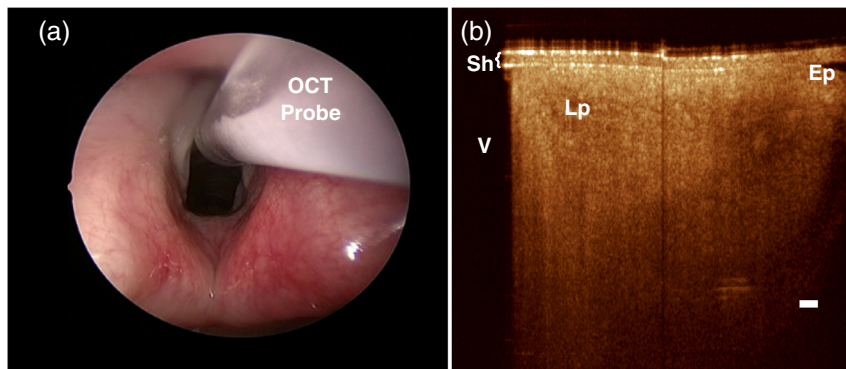


Fig. 6 Healthy 9-year-old male. (a) Intraoperative endoscopy view of the OCT probe within the glottis and (b) corresponding OCT cross section taken of the right vocal fold. Sh, protective sheath; V, ventricle; Ep, epithelium; Lp, lamina propria. Scale bar: 200 μm . Video 3 shows the intraoperative procedure for probe positioning. (Video 3, MOV size 18 MB [URL: <http://dx.doi.org/10.1117/1.JBO.21.1.016007.3>]).

Figure 6(b) is the corresponding OCT image showing the protective sheath (Sh), a very thin squamous epithelium layer (Ep), and the relatively hyperluciscent lamina propria (Lp). Similarly to the normal *ex vivo* sample [Fig. 3(a)], the true vocal fold is void of any subepithelial glandular structures and is much more homogeneous than surrounding tissues.

3.2.1 Nodules

Figure 7 shows images from an 11-year-old female with bilateral vocal fold nodules, symmetrically located on the anterior third of the true vocal fold. Epithelial swelling is noticeable in the intraoperative image {highlighted with black arrows [Fig. 7(a)]}. The OCT image [Fig. 7(b)], captured at the junction of the normal region (Ep1) and nodule's location (Ep2), shows a 30% increase in tissue superficial to the basement membrane, which may indicate the presence of hyperkeratotic squamous epithelium. Similar observations were made for all nodule cases

($n = 3$) viewed throughout this *in vivo* study. The transition region from the epithelium to the lamina propria (white arrow) suggests that the basement membrane undergoes significant thickening. Heterogeneous signal can be observed beneath the epithelial lining [highlighted by * mark in Figs. 7(b) and 7(c)]. This structure might arise from the remodeling of the superficial lamina propria with fibronectin deposition^{34,35} or the presence of edema and amyloid-like material.¹⁰ Within this specific region [Fig. 7(d)], the transition between the epithelium and the basement membrane is more diffuse.

3.2.2 Cysts

Figure 8 shows images from a 12-year-old male with a mucus retention cyst. The intraoperative endoscopic image in Fig. 8(a) reveals a swelled structure on the left vocal fold (identified by black arrows). The OCT section [Fig. 8(b)] shows the presence of a cyst below the epithelial layer. The cyst is characterized by a

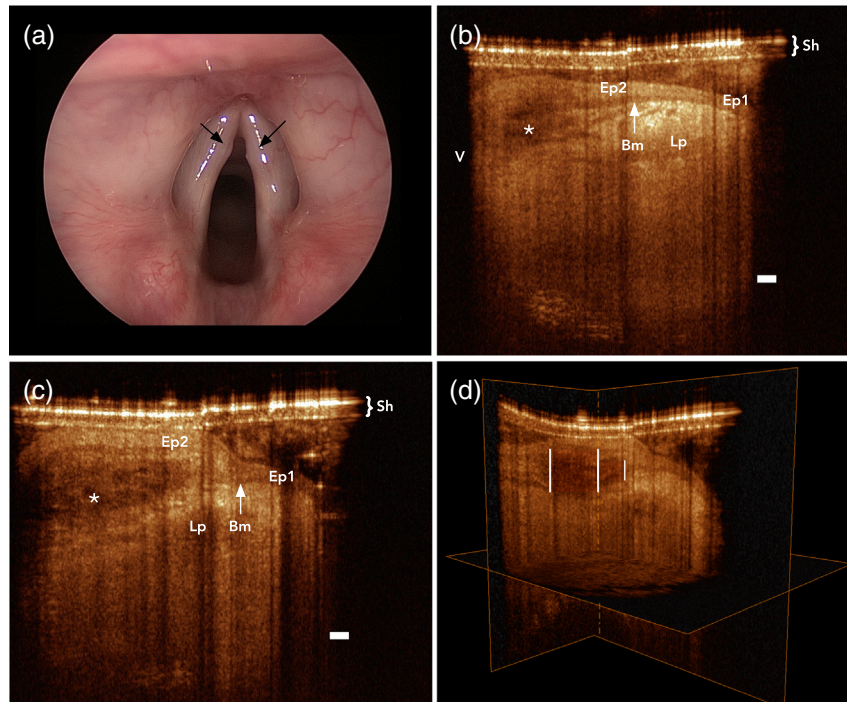


Fig. 7 Eleven-year-old female with bilateral nodules. (a) Intraoperative endoscopy view of the glottis with black arrows pointing at epithelial swelling. Corresponding OCT cross section showing (b) the basement membrane thickening (white arrow) and (c) the apex of the nodule. (d) Video 4 shows a fly-through of the 3-D data set. Sh, protective sheath; Ep1, epithelium location 1; Ep2, epithelium location 2; Bm, basement membrane; Lp, lamina propria; and V, ventricle. Scale bars: 200 μm . (Video 4, MP4 size 8 MB [URL: <http://dx.doi.org/10.1117/1.JBO.21.1.016007.4>]).

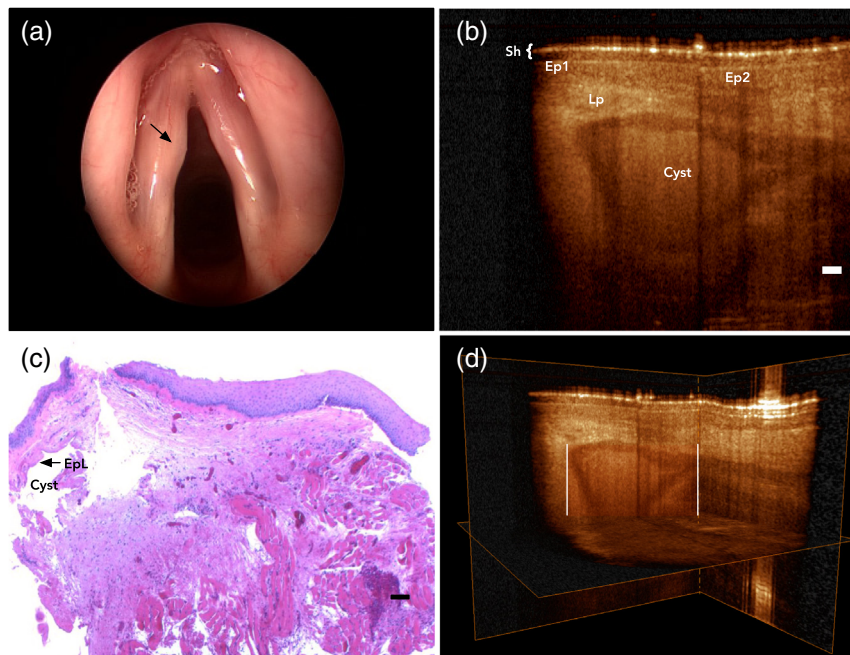


Fig. 8 Twelve-year-old male with cyst. (a) Intraoperative view of the glottis with a black arrow pointing at the epithelial swelling. (b) OCT cross section showing an oval-shaped structure within the lamina propria. (c) Corresponding histological section (H&E staining 100 \times). (d) Video 5 shows the 3-D mucus retention cyst. Sh, protective sheath; Ep1, epithelium location 1; Ep2, epithelium location 2; and Lp, lamina propria. Scale bar: 200 μm . (Video 5, MP4 size 6 MB [URL: <http://dx.doi.org/10.1117/1.JBO.21.1.016007.5>]).

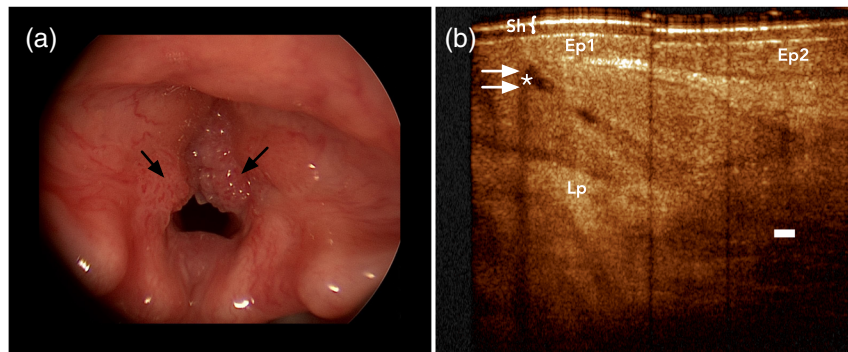


Fig. 9 Three-year-old male with laryngeal papillomatosis. (a) Intraoperative view of the glottis with black arrows highlighting locations of epithelial hyperplasia. (b) OCT cross sections showing significantly irregular epithelial layer invaginating within the lamina propria with a star identifying what could be a large blood vessel. Sh, Protective sheath; Ep1, epithelium location 1; Ep2, epithelium location 2; Lp, lamina propria. Scale bar: 200 μm .

homogenous moderately scattering region surrounded by a low scattering region of $\sim 60 \mu\text{m}$ in thickness. Backscattered signal originating from inside the cyst suggests a content that is not pure liquid, but rather, a turbid fluid. By opposition to the aqueous cyst, which presents with delineated void region [Fig. 4(c)], the mucus retention cyst contains a mixture of protein, mucin, and cellular debris, which is consistent with the turbid appearance of its center. The corresponding histopathology section shown in Fig. 8(c) confirms the presence of a mucus retention cyst with a clearly defined epithelial lining (EpL), consistent with the surrounding boundary seen in the OCT image [Fig. 8(b)]. The 3-D OCT volume acquired permits extraction of the cyst lesion [Fig. 8(d)], which appears as complex oval shape. As with the *ex vivo* specimen, this cyst is not symmetrical and expands on 1 mm on the superior–inferior axis and 2 mm on the anterior–posterior axis and is 1.5-mm deep in the lamina propria.

3.2.3 Laryngeal papillomatosis

Figure 9(a) shows an intraoperative endoscopic image of a 3-year-old patient with multiple warty growths (papillomas) in the anterior commissure. As seen on the corresponding OCT image [Fig. 9(b)], this lesion is associated with a significant increase in epithelial thickness. The epithelial layer is irregular in size (Ep1–Ep2) and invaginations of the epithelium inside the lamina propria can be seen, consistent with epithelial hyperplasia typically seen in papilloma lesions. Figure 9(b) shows an oval-shaped void region (indicated by white arrows) in the epithelial layer, which may correspond to a blood vessel.

4 Discussion

The pediatric vocal fold microarchitecture has not yet been completely elucidated. The invasiveness of current imaging techniques and the rarity of pediatric cadaveric specimens have hindered our current knowledge of this unique and changing anatomical structure. The opportunity to observe the vocal fold beneath the epithelium surface allows for a more thorough investigation of normal and abnormal structures to detect voice pathologies at a stage when appropriate interventions can be applied. Distinguishing between lesions is not always possible through intraoperative endoscopy as mucosal swelling could be indicative of several pathologies and because some lesions may be buried deep within the mucosa. OCT, a noninvasive imaging

technology, adapted to the context of pediatric laryngology could be a promising tool for clinicians as it allows for noninvasive visualization of the microstructure of the vocal fold.

In this study, we developed an intraoperative OCT handheld probe with the aim of imaging pediatric lesions with adequate resolution, field-of-view, contrast, and speed. The modification of a commercial system yielded a compact, robust, and highly stable imaging tool with an imaging range long enough to capture lesions with large topographic variations.

Ex vivo imaging revealed an OCT contrast sufficient to identify boundaries of the epithelium and lamina propria for structural evaluations. It is also allowed establishing a procedure for *in vivo* imaging of the strike zone by navigating from the glandular subglottic region.

In vivo imaging was also facilitated by the long coherence length rapid OCT system, which allowed volumetric acquisition on both left and right strike zones to be acquired within less than 2 min. No technical difficulties occurred during the *in vivo* study. The intraoperative probe used benefited from its ergonomically swappable probe tips, laser engraved marks for positioning, and small size to minimize obstruction of the operative field. The rotational mount added to the probe allowed for rapid and repeatable alignment with the region-of-interest. Additionally, the design allows selecting the imaging plane independently of the scanning angle. This degree of freedom proved to be immensely helpful as we quickly realized that imaging the coronal plane of the vocal fold is key in navigating the vocal fold topography and to acquire consistent imaging areas. However, despite the probe compliance with the system design specifications (imaging with expected resolution, contrast and speed), it still suffers from saturation artifacts (i.e., vertical lines overlapping with the sample) from backreflections from the sterile sheath. The commercially available disposable sheath, which increases our efficiency in the operating room (facilitated sterilization) was not originally designed for OCT imaging. The availability of sheaths made of other materials, such as fluorinated ethylene propylene, would be beneficial to OCT imaging yielding in a higher transmission of near-infrared light.

The handheld probe allowed imaging patients ranging from 3 months to 16 years. For younger patients, the probe needs further miniaturization ($<1.5\text{-mm}$ diameter) to avoid obstructing the airway. This task can be achieved using either smaller GRIN lenses with the current design or with an optical fiber probe. For both cases, this might come at a price of significantly

reducing the field-of-view. However, a smaller field-of-view may still be adequate in younger children as the lesion and vocal fold length are proportionally smaller.

The subsurface 3-D data acquired with OCT was essential in the evaluation of the microanatomy of the lamina propria. Our normal specimens showed a relatively homogeneous signal, void of any glandular-like structures over the depth of the true vocal fold. The epithelium layer showed a relatively constant intensity along the length of the true fold. Its thickness increased, but remained relatively thin from an inferior to superior aspect, which is consistent with the transition from stratified squamous to pseudostratified ciliated epithelial cells. Beneath the epithelial layer, the lamina propria appears hyperluculent relative to epithelium, which may be attributed to the extracellular matrix and loosely packed collagen and elastin fibers that can be found in this region.³⁶ The intensity of the vocal fold relative to the depth seemed to decrease differently along the vocal fold's superior-inferior axis, which is consistent with variations in cellular and fiber densities seen in laryngeal tissues.

For pathological cases, despite a relatively uniform endoscopic representation, OCT images revealed important subsurface variations. For vocal fold nodules, the epithelium layer seemed to be slightly thicker, which might be an indication of hyperplasia or, in some cases, hyperkeratinization. Nodules showed evidence of structural changes just beneath the thickened basement membrane. Cysts are located deeper within the lamina propria and have a complex 3-D shape (i.e., nonspherical). Mucus retention cysts showed a clear turbid region with an epithelial lining while pseudocysts presented with void areas, suggesting a clear aqueous material filling. The extent of these benign lesions is hard to identify with superficial imaging techniques, as well as with 2-D OCT, highlighting the benefit of a 3-D representation. This study was, however, performed on a limited sample set to primarily demonstrate the ability of this probe to image lesions. Imaging of a larger patient cohort is underway to establish a complete set of diagnostic criteria.

The depth of laryngeal papillomatosis lesions, which are seen superficially with intraoperative endoscopy, is revealed under OCT showing an epithelium layer significantly thicker and irregular along the true vocal fold with invaginations within the lamina propria. OCT used jointly with angiolytic lasers could lead to depth controlled treatments to limit scarring of surrounding tissues, and preserve voice to the greatest extent possible. Earlier work focusing on combining OCT and laser therapy was performed in the field of gastroenterology, which could potentially be extended to the use of ablation laser.³⁷⁻⁴⁰

The OCT handheld probe allowed extraction of features of several common benign pediatric lesion types with sufficient contrast, resolution, and penetration depth to give surgeons essential clinical insights to these lesions. Some steps are currently undertaken to further miniaturize the probe in order to allow targeting even younger patients (under 3 months). Further improvements include adding a second modality to investigate molecular contrasts provided by fluorescence,⁴¹ nonlinear contrast,⁴² or spectroscopy.⁴³

5 Conclusion

OCT adapted to the context pediatric laryngology is a promising tool providing valuable structural information to clinicians. We believe that the proposed OCT system, including a 3-D-capable handheld probe, is a stepping-stone in the development of specially designed tools for pediatric laryngology. Noninvasive

assessment of the type and the extent of laryngeal diseases may be very helpful for guiding surgical interventions. Moreover, although this study was focused on pediatric lesion imaging, the OCT probe could be used to image healthy vocal folds for a quantitative study of the development of the lamina propria. A better understanding of this unique organ would further improve the management of pediatric laryngeal diseases.

Acknowledgments

The authors would like to thank Dr. Anjul Loiacono and Dr. Shahidul Islam for their contribution in adapting the VSCEL system for clinical use, as well as Dr. William Faquin, director of the Head and Neck Pathology Unit, for the analysis of histology sections. We further thank Martin Guernon, Yves Leblanc, and Evgueni Babian for the fabrication of custom parts. This research is supported in part by the NSERC Discovery Grant (341555-13).

References

1. P. N. Carding, S. Roulstone, and K. Northstone, "The prevalence of childhood dysphonia: a cross-sectional study," *J. Voice* **20**, 623-630 (2006).
2. D. K. Wilson, *Voice Problems in Children*, Vol. 1, Williams & Wilkins, Baltimore (1987).
3. S. R. Schwartz et al., "Clinical practice guideline: hoarseness (dysphonia)," *Otolaryngol. Head Neck Surg.* **141**, S1-S31 (2009).
4. L. N. Kelchner et al., "Perceptual evaluation of severe pediatric voice disorders: rater reliability using the consensus auditory perceptual evaluation of voice," *J. Voice* **24**, 441-449 (2010).
5. F. Midulla et al., "Flexible endoscopy of paediatric airways," *Eur. Respir. J.* **22**, 698-708 (2003).
6. P. H. Dejonckere et al., "A basic protocol for functional assessment of voice pathology, especially for investigating the efficacy of (phonosurgical) treatments and evaluating new assessment techniques: guideline elaborated by the Committee on Phoniatrics of the European Laryngology," *Eur. Arch. Otorhinolaryngol.* **258**, 77-82 (2001).
7. P. Song, "Assessment of vocal cord function and voice disorders," in *Principles and Practice of Interventional Pulmonology*, Springer, New York (2013).
8. L. L. Swanson and N. J. Soper, *Mastery of Endoscopic and Laparoscopic Surgery*, Wolters Kluwer Health (2013).
9. A. M. Klein et al., "Imaging the human vocal folds in vivo with optical coherence tomography: a preliminary experience," *Ann. Otol. Rhinol. Laryngol.* **115**(4), 277-284 (2006).
10. L. Wallis et al., "Vocal fold nodule vs. vocal fold polyp: answer from surgical pathologist and voice pathologist point of view," *J. Voice* **18**, 125-129 (2004).
11. A. Hantzakos et al., "Exudative lesions of Reinke's space: a terminology proposal," *Eur. Arch. Otorhinolaryngol.* **266**, 869-878 (2009).
12. J. Oates and A. Winkworth, "Current knowledge, controversies and future directions in hyperfunctional voice disorders," *Int. J. Speech Lang. Pathol.* **10**, 267-277 (2008).
13. C. A. Rosen et al., "A nomenclature paradigm for benign midmembranous vocal fold lesions," *Laryngoscope* **122**, 1335-1341 (2012).
14. D. L. Wohl, "Nonsurgical management of pediatric vocal fold nodules," *Arch. Otolaryngol. Head Neck Surg.* **131**, 68-70, discussion 71-72 (2005).
15. C. Boudoux et al., "Preliminary evaluation of noninvasive microscopic imaging techniques for the study of vocal fold development," *J. Voice* **23**, 269-276 (2009).
16. C. Boudoux et al., "Optical microscopy of the pediatric vocal fold," *Arch. Otolaryngol. Head Neck Surg.* **135**, 53-64 (2009).
17. M. J. Hawkshaw, J. B. Sataloff, and R. T. Sataloff, "New concepts in vocal fold imaging: a review," *J. Voice* **27**, 738-743 (2013).
18. D. Huang, E. Swanson, and C. Lin, "Optical coherence tomography," *Science* **254**, 1178-1181 (1991).
19. A. V. Shakhov et al., "Optical coherence tomography monitoring for laser surgery of laryngeal carcinoma," *J. Surg. Oncol.* **77**, 253-258 (2001).

20. J. A. Burns et al., "Imaging the mucosa of the human vocal fold with optical coherence tomography," *Ann. Otol. Rhinol. Laryngol.* **114**, 671–676 (2005).
21. J. Gracia et al., "Using attenuation coefficients from optical coherence tomography as markers of vocal fold maturation," *Laryngoscope* (2015).
22. B. J. F. Wong et al., "In vivo optical coherence tomography of the human larynx: normative and benign pathology in 82 patients," *Laryngoscope* **115**, 1904–1911 (2005).
23. A. G. Bibas et al., "3-D optical coherence tomography of the laryngeal mucosa," *Clin. Otolaryngol.* **29**, 713–720 (2004).
24. W. B. Armstrong et al., "Optical coherence tomography of laryngeal cancer," *Laryngoscope* **116**, 1107–1113 (2006).
25. A. Klein et al., "Imaging the human vocal folds in vivo with optical coherence tomography: a preliminary experience," *Ann. Otol. Rhinol. Laryngol.* **115**(4), 277–284 (2006).
26. J. A. Burns et al., "Polarization-sensitive optical coherence tomography imaging of benign and malignant laryngeal lesions: an in vivo study," *Otolaryngol. Head Neck Surg.* **145**, 91–99 (2011).
27. K. H. Kim et al., "In vivo 3D human vocal fold imaging with polarization sensitive optical coherence tomography and a MEMS scanning catheter," *Opt. Express* **18**, 14644–14653 (2010).
28. J. M. Ridgway et al., "Imaging of the pediatric airway using optical coherence tomography," *Laryngoscope* **117**, 2206–2212 (2007).
29. V. Volgger et al., "Long-range Fourier domain optical coherence tomography of the pediatric subglottis," *Int. J. Pediatr. Otorhinolaryngol.* **79**, 119–126 (2015).
30. G. K. Sharma et al., "Long range optical coherence tomography of the neonatal upper airway for early diagnosis of intubation-related subglottic injury," *Am. J. Respir. Crit. Care Med.* **192**(12), 1504–1513 (2015).
31. V. Jayaraman et al., "High-sweep-rate 1310 nm MEMS-VCSEL with 150 nm continuous tuning range," *Electron. Lett.* **48**, 867–869 (2012).
32. M. Hirano, "Phonosurgery: basic and clinical investigations," *Otologia* **21**(Suppl. 1), 239–442 (1975).
33. R. B. Nunes et al., "Clinical diagnosis and histological analysis of vocal nodules and polyps," *Braz. J. Otorhinolaryngol.* **79**, 434–440 (2013).
34. S. D. Gray, S. S. Pignatari, and P. Harding, "Morphologic ultrastructure of anchoring fibers in normal vocal fold basement membrane zone," *J. Voice* **8**, 48–52 (1994).
35. R. H. G. Martins et al., "Vocal fold nodules: morphological and immunohistochemical investigations," *J. Voice* **24**, 531–539 (2010).
36. S. D. Gray et al., "Biomechanical and histologic observations of vocal fold fibrous proteins," *Ann. Otol. Rhinol. Laryngol.* **109**, 77–85 (2000).
37. B. J. Vakoc, G. J. Tearney, and B. E. Bouma, "Real-time microscopic visualization of tissue response to laser thermal therapy," *J. Biomed. Opt.* **12**, 020501 (2007).
38. M. Villiger et al., "Injury depth control from combined wavelength and power tuning in scanned beam laser thermal therapy," *J. Biomed. Opt.* **16**, 118001 (2011).
39. H. W. Baac, N. N. Uribe-Patarroyo, and B. E. Bouma, "High-energy pulsed Raman fiber laser for biological tissue coagulation," *Opt. Express* **22**, 7113 (2014).
40. K. Beaudette et al., "Laser tissue coagulation and concurrent optical coherence tomography through a double-clad fiber coupler," *Biomed. Opt. Express* **6**, 1293 (2015).
41. L. Scolaro et al., "Molecular imaging needles: dual-modality optical coherence tomography and fluorescence imaging of labeled antibodies deep in tissue," *Biomed. Opt. Express* **6**, 1767 (2015).
42. M. Strupler et al., "Nonlinear Microscopy of the Vocal Folds," B. Wong and J. Ilgner, Eds. (2015).
43. R. G. Lord et al., "A 1060 nm double clad fiber coupler for combined optical coherence tomography and endoscopy," *Proc. SPIE* **4** (2016).

Fouzi Benboujja is a graduate student in the Department of Biomedical Engineering at Ecole Polytechnique of Montreal under the supervision of Professor Caroline Boudoux. His research focuses on developing noninvasive optical imaging tools to improve our current knowledge of vocal fold microanatomy.

Biographies for the other authors are not available.